Rational design of carbon-doped carbon nitride/$Bi_{12}O_{17}Cl_2$ Composites: A Promising Candidate Photocatalyst for boosting visible-light driven photocatalytic degradation of tetracycline

Chengyun Zhou[1], Cui Lai[1], Piao Xu[1], Guangming Zeng[*], Danlian Huang[*], Zhihao Li, Chen Zhang, Min Cheng, Liang Hu, Jia Wan, Fei Chen, Weiping Xiong, Rui Deng

College of Environmental Science and Engineering, Hunan University and Key Laboratory of Environmental Biology and Pollution Control (Hunan University), Ministry of Education, 8 South Lushan Road, Yuelu District, Changsha 410082, P.R. China

∗ Corresponding author at: College of Environmental Science and Engineering, Hunan University, Changsha, Hunan 410082, China.

Tel.: +86–731– 88822754; fax: +86–731–88823701.

E-mail address: zgming@hnu.edu.cn (G.M. Zeng), huangdanlian@hnu.edu.cn (D.L. Huang).

1 These authors contribute equally to this article.

Abstract

Many recent advances based on 2D materials have opened new possibilities in photocatalysis. In this study, a new 2D semiconductor composite consisting of carbon-doped carbon nitride (denoted as CCN) layers and $Bi_{12}O_{17}Cl_2$ layers was designed via an in-situ method. Supramolecular chemistry approach was employed to form CCN by using the hydrogen bonded melamine-cyanuric acid and barbituric acid complex, and $Bi_{12}O_{17}Cl_2$ layers were obtained by using a moderate solvothermal method**.** CCN/$Bi_{12}O_{17}Cl_2$ composite photocatalyst had superior photocatalytic activity for degrading antibiotic tetracycline (TC) under visible light irradiation. The degradation rate constant of 20%CCN/$Bi_{12}O_{17}Cl_2$ is 0.0409 min^{-1}, which is approximately 2.9, 1.5, and 32.1 folds than that of pristine $Bi_{12}O_{17}Cl_2$, CCN, and BiOCl, respectively. Photocurrent response and electrochemical impedance spectroscopy showed that CCN/$Bi_{12}O_{17}Cl_2$ composite has high photogenerated charge carrier separation efficiency. According to the radical species trapping experiments and electron spin resonance analyses, $\cdot O_2^-$ and h^+ were confirmed to be the mainly active species involved in the degradation of organic pollutants. The enhanced photocatalytic activities of CCN/$Bi_{12}O_{17}Cl_2$ could be ascribed to enhanced charge separation. It is expected that the CCN/$Bi_{12}O_{17}Cl_2$ composite could be utilized as visible light phtocatalyst for other environmental applications.

Keywords: Carbon-doped carbon nitride, $Bi_{12}O_{17}Cl_2$, Semiconductor composites, Visible light photocatalysis, Antibiotic degradation

INTRODUCTION

In the past few decades, the rapid development of society has caused some problems like energy shortage and environmental deterioration.[1-5] The emerging environmental contaminants such as phenols, pesticides and antibiotics in water cycling system, especially in drinking water have posed serious threats to the organisms and human beings' health even at low concentrations.[6-10] The U.S. Environment Protection Agency has listed them as priority control contaminants.[11-15] Many effective treatments have been developed to address these serious issues, including biological treatment,[16-17] adsorption,[18-23] photocatalysis[24] and so on. Biological degradation has been shown to be a promising method for removal of organics from wastewater as some specific bacteria can convert these organics to inorganic molecules with less secondary pollution when compared with adsorption methods.[25-27] However, biological treatment requires a relatively long period time.[28-29] Different with them, photocatalytic degradation technology could utilize solar energy to achieve the mineralization of contaminated organics.

Semiconductor photocatalyst has great potential in resolving environmental problems caused by organic pollutants.[7, 30] To realizing this target, the key point in is to search for the appropriate photocatalysts with sufficient sunlight absorption and efficient photo-induced charge separation.[31-32] Bismuth oxychloride (BiOCl), a wide-band-gap (about 3.2 eV) ternary semiconductor, has attracted considerable attention owing to its layer structure, high chemical and optical stability.[33] BiOCl could not utilize visible light, but it could construct the desired bandgap semiconductors where band gap can be adjusted by ratio of Cl and O, such as $Bi_{12}O_{17}Cl_2$. $Bi_{12}O_{17}Cl_2$ has a unique layered structure, excellent photophysical and chemical properties. Also, this material is nontoxic and chemically stable. These fascinating properties have attracted a great

deal of research interest and can be applied to environmental remediation.[34] It has been employed to oxidize benzyl alcohol and degrade bisphenol A under visible light.[35-36] Though a number of $Bi_{12}O_{17}Cl_2$ based composite photocatalysts have been synthesized, such as BiOI@$Bi_{12}O_{17}Cl_2$,[37] $Bi_{12}O_{17}Cl_2$/β-Bi_2O_3,[38] and BiOCl-$Bi_{12}O_{17}Cl_2$.[39] Nevertheless, $Bi_{12}O_{17}Cl_2$ composited with non-metal photocatalysts has not been achieved. In addition, as reported by Zhang et al., the electrons originating from $Bi_{12}O_{17}Cl_2$ were driven by internal electric field (IEF) between (Cl_2) and ($Bi_{12}O_{17}$), and further transferred to other semiconductors.[40] This hypothesis is good for us to build an efficient photocatalysis system.

Polymeric graphitic carbon nitride (g-C_3N_4) with conjugated system attracts tremendous scientific interest owing to its excellent visible light activity, and high chemical stability for water splitting, CO_2 oxidation, contaminant degradation.[41-43] Wang et al. reported that g-C_3N_4 could be applied for H_2 production from water under visible light irradiation.[44] Many researchers have utilized g-C_3N_4 to contaminant degradation under visible light.[45] However, the low quantum efficiency, ultrafast recombination of photoinduced charge carriers and insufficient sunlight absorption currently has limited the practical application of g-C_3N_4.[46-49] Fortunately, these shortcomings might be overcame through fabricating heterojunctions with other photocatalysts, such as TiO_2,[50] ZnO,[24] Bi_2WO_6,[51-53] and $BiVO_4$.[54-58] Motivated by flourish studies on heterostructures, we focused the work on the heterojunction between g-C_3N_4 and $Bi_{12}O_{17}Cl_2$ due to the good optical properties of g-C_3N_4 and well electrical conductivity of $Bi_{12}O_{17}Cl_2$ layer.

Herein, the $Bi_{12}O_{17}Cl_2$ hybridized carbon-doped g-C_3N_4 (denoted as CCN) composites with different proportions were fabricated in this study. The obtained composites were denoted as x% CCN/$Bi_{12}O_{17}Cl_2$, where x refers to the weight percentages of CCN with $Bi_{12}O_{17}Cl_2$. The

microstructure, optical properties and photoelectric performances of CCN/$Bi_{12}O_{17}Cl_2$ were investigated. The degradation kinetics of prepared photocatalyst on commonly antibiotics pollutant (i.e., tetracycline) was explored under the irradiation of visible light. It is fascinating to find that CCN/$Bi_{12}O_{17}Cl_2$ exhibits outstanding photocatalytic activity toward degradation of tetracycline (TC) compared with pristine $Bi_{12}O_{17}Cl_2$. The band gap structure and proposed mechanism were proposed.

EXPERIMENTAL SECTION

Preparation of Catalysts. Melamine ($C_3H_6N_6$), cyanuric acid ($C_3H_3N_3O_3$), and barbituric acid ($C_3H_4N_2O_3$) were received from Sinopharm Chemical Reagent Co., Ltd (Shanghai, China). All chemicals used in this study were reagent grade and used without further purification. The synthesized procedure was according to our previous report.[59] The CCN samples were prepared by using 1 mmol of melamine, 1 mmol of cyanuric acid and 0.1 mmol of barbituric acid in 100 mL of ethanol. Then the mixture was sonication for 1 h and stirred at ambient temperature for another 2 h. The mixture was dried and calcined at 550 °C for 4 h with a heating rate of 3.6 °C min^{-1}. The obtained powder was centrifuged, washed and dried. Then the yellow resultant carbon-doped carbon nitride (CCN) was obtained. The typical bulk carbon nitride (CN) was obtained by using melamine at 550 °C for 4 h with a heating rate of 3.6 °C min^{-1}.

Bismuth nitrate pentahydrate ($Bi(NO_3)_3{\cdot}5H_2O$), ammonium chloride (NH_4Cl), ethylene glycol (EG), and sodium hydroxide (NaOH) were received from Sinopharm Chemical Reagent Co., Ltd (Shanghai, China). The $Bi_{12}O_{17}Cl_2$ was fabricated by a previously reported method with some modifications.[60-61] In a typical method, 2.5 mmol of $Bi(NO_3)_3{\cdot}5H_2O$ was dissolved in a 10 mL of EG. Then the above solution was added into 60 mL of distilled water containing 6 mmol of

NH_4Cl and 20 mmol of NaOH. The mixture was heated at 160 °C for 12 h. The obtained resultant was collected and washed with distilled water and ethanol and dried.

The CCN/$Bi_{12}O_{17}Cl_2$ composite was fabricated by an in situ procedure. First, the as-prepared was dispersed into 50 mL of methanol, and kept under sonication for 1 h to promote the dispersion of CCN. Then, a certain amount of $Bi_{12}O_{17}Cl_2$ was added into the above mixture, and under sonication for another 1h. After that, the mixture was stirred for 12 h. Then the mixture was centrifuged, and washed three times with ethanol and distilled water. The sample was dried and further treated at 120 °C for 2h in air to enhance the interaction between $Bi_{12}O_{17}Cl_2$ and the carbon nitride matrix. The samples were denoted as X CCN/$Bi_{12}O_{17}Cl_2$ (X is the mass ratio of CCN to samples). They were 5% CCN/$Bi_{12}O_{17}Cl_2$, 10% CCN/$Bi_{12}O_{17}Cl_2$, 20% CCN/$Bi_{12}O_{17}Cl_2$, and 30% CCN/$Bi_{12}O_{17}Cl_2$.

Characterization Methods. The structure of samples was examined by high-resolution scanning electron microscopy (HR-SEM) (FEI Helios NanoLab 600i dual beam system) and transmission electron microscopy (HAADF-STEM, FEI Tecnai G2F20 S-TWIN). The crystal phases of the samples were achieved from a X-ray diffractometer (D/max-2500; Rigaku, Japan) using Cu *Kα* radiation (λ = 0.15406 nm). The scan region of 2θ was from 10º to 80º. The binding energy of the as-prepared samples was investigated by X-ray photoelectron spectra (XPS, ESCALAB 250Xi spectrometer, Thermo Fisher, USA). Fourier transformed infrared (FTIR, FTS-6000) spectra of samples were obtained. The UV-vis diffuse reflectance spectra (DRS) of samples were measured on UV-vis spectrophotometer (Cary 300, USA) with $BaSO_4$. The electron spin resonance (ESR) signals of radicals spin-trapped by trapping reagent 5,5-dimethyl-lpyrroline N-oxide (DMPO) was collected on Bruker ER200-SRC spectrometer under visible light

irradiation (> 420 nm).

Photocatalytic Experiments. The photocatalytic degradation activities were evaluated by the degradation of TC under a 300 W Xe lamp (CELHXF300, Beijing, China) irradiation with a 420 nm cutoff filter. The degradation pollutants were 50 mL TC aqueous solution with the initial concentration of 20 mg L^{-1}. The dosage of photocatalyst was 1 g L^{-1}. Before irradiation, the solution was magnetically stirred for 1 h in dark to reach the equilibrium between adsorption and desorption. Subsequently, the mixture was exposed to visible light. 3 mL of solution was taken out at given time interval and the particles were separated by centrifugation and filtrated. The concentration of TC was measured by the UV-vis spectrophotometer and the maximum peak was 357 nm.

Electrochemical Measurements. The electrochemical measurements were realized in a three-electrode system on an electrochemical workstation (CHI 660D, China). The working electrode was prepared on fluorine-doped tin oxide (FTO) glass, which was cleaned with ethanol and dried. 10 mg sample was dispersed in 2 mL dimethyl formamide by sonication for 0.5 h. Then the slurry was spread onto pretreated FTO glass, and dried in a vacuum oven for 2 h at 120 °C. The platinum plate as the counter electrode and the Ag/AgCl electrode as the reference electrode were used in three-electrode system. Na_2SO_4 solution (0.2 M) was used as the measure system aqueous electrolyte. The photocurrent responses of the samples as light on and off were measured at 0 V. Visible light was obtained by the 300 W xenon lamp with a 420 nm cutoff filter. In addition, the Mott-Schottky plots and electrochemical impedance spectroscopy (EIS) were also performed in this system.

RESULTS AND DISCUSSION

Catalysts Characterization. The morphology and compositions of $Bi_{12}O_{17}Cl_2$, CCN, and CCN/$Bi_{12}O_{17}Cl_2$ were determined by SEM with the energy dispersive spectrometer (EDS) analysis. As shown in Figure 1a, $Bi_{12}O_{17}Cl_2$ possessed nanosheet structure. The CCN exhibited nanosheets with stacked layers and smooth surface, as depicted in Figure 1b. As displayed in Figure 1c-d, the CCN nanosheet integrates with 2D $Bi_{12}O_{17}Cl_2$ nanosheet effectively, which may pose large effect on the photocatalytic activity. Meanwhile, the EDS mapping were utilized to identify the elements of CCN/$Bi_{12}O_{17}Cl_2$ in Figure 1e-i. The elements of Bi, O, Cl, C, and N are distributed on the surface of the sample, indicating that the CCN/$Bi_{12}O_{17}Cl_2$ is composed of CCN and $Bi_{12}O_{17}Cl_2$ component. Further detailed morphology and crystallography of the samples were studied by TEM in Figure 2. As shown in Figure 2a and 2b, the layered structure of CCN and the nanosheet structure of $Bi_{12}O_{17}Cl_2$ were found, respectively. The length and width of $Bi_{12}O_{17}Cl_2$ nanosheet were 200-400 nm and 40-100 nm, respectively. The $Bi_{12}O_{17}Cl_2$ nanosheets disperse on the surface of CCN uniformly, which would effectively enhance the interaction between them (Figure 2c). The CCN/$Bi_{12}O_{17}Cl_2$ was further studied by HRTEM in Figure 2d. It was observed that the lattice distance was 0.338 nm, corresponding to the (115) facets of $B_{12}O_{17}Cl_2$. The CCN nanosheets were employed as the substrate of $B_{12}O_{17}Cl_2$, and marked in Figure 2c-d. The interaction of $B_{12}O_{17}Cl_2$ and CCN enhanced the separation efficiency of photogenerated carriers.

The crystal structures and phase purity of pristine CCN, $Bi_{12}O_{17}Cl_2$, and all the CCN/$Bi_{12}O_{17}Cl_2$ samples were determined by X-ray diffraction (XRD). As shown in Figure 3a, the peak of CCN nanosheets located at 13.1^o and 27.2^o were ascribed to the (100) and (002) planes, respectively. The (002) peak of CCN obviously became weaker and broader compared to the bulk CN (in Figure S1), indicating that the reduced layer thickness.[62] The main peaks of $Bi_{12}O_{17}Cl_2$ at

24.57°, 29.46°, and 32.97° could be ascribed to (115), (117), and (200) crystal planes of $Bi_{12}O_{17}Cl_2$, respectively, which can be indexed with the standard phase of $Bi_{12}O_{17}Cl_2$ (JCPDS card no. 37-0702).[60] As can be seen from the patterns of CCN/$Bi_{12}O_{17}Cl_2$ composites, the characteristic peaks of $Bi_{12}O_{17}Cl_2$ with different amounts of CCN are in agreement with the XRD patterns of pristine $Bi_{12}O_{17}Cl_2$, which indicating the keep of the $Bi_{12}O_{17}Cl_2$ structure. With the increase in the CCN amount, the intensity of typical diffraction peak (002) was increased in the CCN/$Bi_{12}O_{17}Cl_2$. These results indicated that the CCN/$Bi_{12}O_{17}Cl_2$ samples were successful obtained.

The surface bond structures of the as-prepared samples were studied by FT-IR. Figure 3b shows the spectra of CCN, $Bi_{12}O_{17}Cl_2$, and CCN/$Bi_{12}O_{17}Cl_2$ composite. The bands in the 400-600 regions can be ascribed to the stretching mode of Bi-O units in the $Bi_{12}O_{17}Cl_2$. In the FT-IR spectrum of CCN, the peak at 810 cm^{-1} can be associated with the bending modes C-N heterocycles. The peaks at 1247 cm^{-1}, 1324 cm^{-1}, 1414 cm^{-1} and 1572 cm^{-1} can be attributed to the aromatic C-N stretching. The peak at 1632 cm^{-1} was related to the C=N stretching vibration modes.[63] All the characteristic absorption peaks of $Bi_{12}O_{17}Cl_2$ and CCN were observed in the CCN/$Bi_{12}O_{17}Cl_2$ composite, indicating that $Bi_{12}O_{17}Cl_2$ successfully composited with CCN, which was consistent with XRD results.

The surface elemental compositions and binding state of CCN/$Bi_{12}O_{17}Cl_2$ composite were evaluated by XPS analyses in Figure 4. Elements like C, Bi, O, N, and Cl were detected in the spectrum of CCN/$Bi_{12}O_{17}Cl_2$ (Figure 4a). As shown in Figure 4b, the two peaks located at 158.9 and 164.3 eV refer to Bi $4f_{7/2}$ and Bi $4f_{5/2}$, respectively, which indicated that the Bi^{3+} species was in CCN/$Bi_{12}O_{17}Cl_2$. The Cl 2p peak of CCN/$Bi_{12}O_{17}Cl_2$ can be separated into two peaks at 199.6 and 198.1 eV owing to the Cl $2p_{1/2}$ and Cl $2p_{3/2}$, respectively (Figure 4c). As for O 1s peak, it can

be separated into two peaks. The peak located at 530.9 eV may belongs to the O-H bond absorbed on the surface and another peak at 529.8 eV may results from the lattice Bi-O-Bi bond (Figure 4d). In Figure 4e, the peaks of C 1s at 284.5 and 287.8 eV are found, which corresponding to C-C bonding and N=C-N bonding, respectively. The N 1s peak divides into two peaks, which was located at 398.3 eV and 400.1 eV (Figure 4f). The peak at 398.3 eV was owing to the triazine rings (C=N-C) and 400.1 eV was ascribed to the tertiary nitrogen (N-C_3).[60] Additionally, the XPS of bulk CN, CCN and $Bi_{12}O_{17}Cl_2$ were shown in Figure S2. The above results confirm the co-existence of CCN and $Bi_{12}O_{17}Cl_2$ in the composites. In addition, the C/N molecular molar ratio of the sample was summarized in Table S1. The mass ratio of CN was 0.66, while the CCN was 0.78. This evidence indicated the presence of carbon doping in CCN.

Optical Properties and Electrochemical analysis. The UV–Vis DRS spectra of $Bi_{12}O_{17}Cl_2$, CCN, and different mass ratios of CCN/$Bi_{12}O_{17}Cl_2$ composites were shown in Figure 5a. The pristine $Bi_{12}O_{17}Cl_2$ has an absorption edge at about 520 nm, and meanwhile the absorption edge of CCN appeared at about 560 nm. The band gap of the samples can be calculated with the formula $\alpha h\nu = A\,(h\nu - E_g)^{n/2}$, where α, h, ν, A, and E_g are the absorption coefficient, Planck's constant, light frequency, a constant, and band gap energy, respectively.[50, 64] The n constant represents the semiconductor transition.[36, 65] The optical transition of $Bi_{12}O_{17}Cl_2$ and CCN were indirect and direct, respectively. The changes of ($\alpha h\nu$) as a function of the energy of incident photons ($h\nu$) are depicted in Figure 5b. The band gaps of $Bi_{12}O_{17}Cl_2$ and CCN were 2.33 eV and 2.21 eV, respectively. Compared with pristine $Bi_{12}O_{17}Cl_2$, the CCN/$Bi_{12}O_{17}Cl_2$ photocatalyst had an enhanced absorption as the amount of CCN increased.

The photocurrent response of sample was used to certify the efficiency separation of

photogenerated electrons-holes pairs.[66] As shown in Figure 6a, the photocurrent responses of CCN, $Bi_{12}O_{17}Cl_2$ and CCN/$Bi_{12}O_{17}Cl_2$ at light on and off were stable and reversible. The photocurrent of CCN/$Bi_{12}O_{17}Cl_2$ was about 3 times higher than that of the pristine $Bi_{12}O_{17}Cl_2$. The separation efficiency of charge can be further investigated by the electrochemical impedance spectroscopy (EIS). A smaller arc radius in EIS represents a more efficient separation of charge. The EIS Nyquist plots of $Bi_{12}O_{17}Cl_2$ and CCN/$Bi_{12}O_{17}Cl_2$ were presented in Figure 6b. The arc radius of CCN/$Bi_{12}O_{17}Cl_2$ was smaller than that of $Bi_{12}O_{17}Cl_2$, which suggested that CCN/$Bi_{12}O_{17}Cl_2$ had high efficiency of charges than $Bi_{12}O_{17}Cl_2$. These results indicated that interaction was existed in the interface of CCN and $Bi_{12}O_{17}Cl_2$, which suitable for the separation of photogenerated carriers.

Photocatalytic activity. The photocatalytic activities of $Bi_{12}O_{17}Cl_2$, CCN, and CCN/$Bi_{12}O_{17}Cl_2$ composites were evaluated for the degradation of TC. TC is a colorless and refractory pollutant. Figure 6a shows the degradation efficiency of TC as a function of time. Before irradiation, adsorption/desorption equilibrium between the photocatalyst and contaminants in aqueous solution was reached in 60min (Table S2). In Figure 7a, the degradation of TC aqueous solution was negligible without photocatalyst, indicating that the TC is stable under visible light irradiation. The removal of TC with BiOCl, $Bi_{12}O_{17}Cl_2$ and CCN in 1h irradiation was 8%, 54%, and 82%, respectively. All of CCN/$Bi_{12}O_{17}Cl_2$ composites showed superior degradation activities compared to the pristine CCN and $Bi_{12}O_{17}Cl_2$, which can be ascribed to the interaction of composites. When the content of CCN is 20%, the as-prepared composites exhibited the highest photocatalytic activity, and the efficiency was 94% in 1 h. However, Excess CCN would offer as the recombination centers of electron-hole pairs and hindered the light absorption of $Bi_{12}O_{17}Cl_2$, leading to a less photocatalytic activity. Therefore, the photocatalytic activity of CCN/$Bi_{12}O_{17}Cl_2$

composites decreased when the content of CCN was increased to 30%.

In addition, the mechanical mixture of CCN and $Bi_{12}O_{17}Cl_2$ with a 20% mass ratio showed lower photocatalytic activity than that of 20% CCN/$Bi_{12}O_{17}Cl_2$. To further studied the kinetic behaviors of the pollutants degradation in the CCN/$Bi_{12}O_{17}Cl_2$, the TC degradation data were further investigated by applying the L-H model. As presented in Figure S4, all of them fitting well with the pseudo-first-model. Furthermore, the reaction rate constant and degradation rate for TC were shown in Table 1. The 20% CCN/$Bi_{12}O_{17}Cl_2$ composite displayed the fastest reaction rate in degradation of TC with the apparent rate constants of 0.0409 min^{-1}. The k values of all the composites were higher than those of pure CCN and $Bi_{12}O_{17}Cl_2$. Figure S5 exhibited the photocatalytic degradation activity of TC by bulk CN, CCN, bulk CN/$Bi_{12}O_{17}Cl_2$, and CCN/$Bi_{12}O_{17}Cl_2$ under visible light irradiation. Obviously, the CCN and CCN/$Bi_{12}O_{17}Cl_2$ showed much higher photocatalytic activity than bulk CN and bulk CN/$Bi_{12}O_{17}Cl_2$, respectively. As can be seen in Table S3, the BET specific surface area of CCN was 179.03 $m^2 g^{-1}$, which was about 13 times of the bulk CN (13.55 $m^2 g^{-1}$). Thus CCN could provide more active sites for photocatalytic reaction, leading to the photocatalytic activity enhanced.

From the viewpoint of degradation efficiency and practical application, 20% CCN/$Bi_{12}O_{17}Cl_2$ was selected to degrade TC. Effects of initial TC concentration (5, 10, 20, 30, and 40 mg L^{-1}) on the photocatalyst activities were investigated Figure 6b. It was found that the removal efficiency has dropped by increasing the initial TC concentration. The efficiency declined from 94% to 77% in 1h irradiation, while the concentration of TC increased from 5 to 40 mg L^{-1}. It can be said that a higher concentration of TC could decrease the photo-generation of the reactive oxygen species and lead to fewer photons arriving at the surface of the photocatalyst. The result suggested that

lower TC concentration was suitable to obtain the higher removal efficiency. Consequently, dilution was essential in the pretreatment of practical wastewater treatment.

批注 [zcy1]: 改到这里

TC has auto-fluorescence because of its rigid structure.[67] To further explore the degradation and mineralization property of as-prepared CCN/$Bi_{12}O_{17}Cl_2$, 3D EEMs technology was employed. As shown in Figure 7, TC samples mappings were collected in both adsorption and photodecomposition process with CCN/$Bi_{12}O_{17}Cl_2$ under visible light degradation. According to previous studies, two predominant peaks (peak A at λex/λem = (305-330 nm)/(430-450 nm), and peak B at λex/λem = (240-250 nm)/(435-450 nm)) would appear when TC molecules began to decompose . The two peaks could be explained to the humic acids-like and fulvic acids-like fluorescence region, respectively. As shown in Figure 7a-b, no fluorescence signals were observed, indicating that TC molecules were not decomposed in the process of adsorption. With the increase of irradiation time from 30 min to 60 min, the fluorescence intensity increased (Figure7c-d). When the time reaches 120 min, the fluorescence intensity decreased obviously, indicating that the humic acids-like matter and fulvic acids-like matter had been degraded (Figure7f). This result also suggests that the CCN/$Bi_{12}O_{17}Cl_2$ exhibited high mineralization ability to TC.

The photostability of CCN/$Bi_{12}O_{17}Cl_2$ was also evaluated. As presented in Figure S5, after four cycles, the photocatalytic activity of CCN/$Bi_{12}O_{17}Cl_2$ exhibited no obvious reduction, indicating the good stability of CCN/$Bi_{12}O_{17}Cl_2$. Furthermore, the chemical stability of the fresh and used samples was further characterized by FT-IR spectra in Figure S6. The XRD peaks of used CCN/$Bi_{12}O_{17}Cl_2$ were consistent with the fresh CCN/$Bi_{12}O_{17}Cl_2$ in Figure S7. Therefore, it can be said that the CCN/$Bi_{12}O_{17}Cl_2$ has excellent photocatalytic activity and good stablity in the

photocatalytic degradation of pollutants.

Possible Degradation Mechanism. To elucidate the reactive radicals of the 20% CCN/$Bi_{12}O_{17}Cl_2$ on the degradation of TC under visible light irradiation during the photocatalytic process, the active species trapping experiment was systematically investigated by using isopropanol (IPA), benzoquinone (BQ) and EDTA-2Na, which are acted as effective •OH, $•O_2^-$, and holes scavengers, respectively. As shown in Figure 9a and Figure 9b, the activity of CCN/$Bi_{12}O_{17}Cl_2$ under visible light irradiation causes a dramatic change by the addition of BQ and EDTA-2Na, suggesting that $•O_2^-$ and holes are the two main oxidative species. However, the activity of CCN/$Bi_{12}O_{17}Cl_2$ has been slightly changed with the addition of IPA, suggesting that •OH radical played an assistant role in the photocatalytic degradation of TC over photocatalyst. To investigate the role of dissolved oxygen in the degradation process, the CCN/$Bi_{12}O_{17}Cl_2$ activities were tested in air and N_2 saturated suspensions. The rate of degradation was decreased from 94% to 33% in the N_2 saturation. More dissolved oxygen was beneficial to the process of photocatalytic degradation, which indicated that oxygen is a necessary medium in forming super oxygen free radical. These results agree with the above reactive radical test.

The above obtained results were further confirmed by ESR spin-trap measurements which were performed for identifying reactive radicals of CCN, $Bi_{12}O_{17}Cl_2$ and CCN/$Bi_{12}O_{17}Cl_2$. DMPO was employed as a spin trap to capture •OH and $•O_2^-$. As shown in Figure 9c and 9d, no ESR signal of the samples has detected in blank condition. In the Figure 9c, upon visible-light irradiation for 8 min, A stronger signal was produced in CCN/$Bi_{12}O_{17}Cl_2$ than $Bi_{12}O_{17}Cl_2$ and CCN, suggesting more $•O_2^-$ was generated under irradiation. Meanwhile, in the Figure 9d, a four-line spectrum with 1:2:2:1 was observed obviously in CCN/$Bi_{12}O_{17}Cl_2$, which were identified

as the characteristic peaks of •OH. The peak of •OH in $Bi_{12}O_{17}Cl_2$ was also detected, but it was weaker than CCN/$Bi_{12}O_{17}Cl_2$. The results of ESR analysis are consistent with the results of the radicals trap experiments.

To further studied the mechanisms of photogenerated electrons and holes, the conduction band (CB) and valence band (VB) positions of pure CCN and $Bi_{12}O_{17}Cl_2$ should be confirmed.[51, 68] Mott–Schottky analysis were utilized to measure the flat band potential of the pure CCN and $Bi_{12}O_{17}Cl_2$ at frequency of 1000 Hz (Figure 10a). The flat band potential of CCN was calculated to be -0.47 V and the $Bi_{12}O_{17}Cl_2$ was −0.44 V versus the Ag/AgCl electrode (SCE), which were −0.27 V and −0.24 V versus the normal hydrogen electrode (NHE).[52, 65, 69-70] In addition, the VB-XPS spectra of CCN and $Bi_{12}O_{17}Cl_2$ were shown in Figure 10b. For CCN and $Bi_{12}O_{17}Cl_2$, it can be seen that the gap between the VB and Fermi level were 2.08 and 1.80 eV, respectively. It is known that the flat potential was equal to Fermi level for n-type semiconductor. So the VB positions of CCN and $Bi_{12}O_{17}Cl_2$ were 1.81 and 1.56 eV respectively. According to the Figure 5b, the band gap of the CCN and $Bi_{12}O_{17}Cl_2$ was calculated to 2.21 and 2.33 eV, respectively. Consequently, the CB positions of CCN and $Bi_{12}O_{17}Cl_2$ were -0.40 and -0.77 eV, respectively.

Based on the above results, the mechanism of CCN/$Bi_{12}O_{17}Cl_2$ composites on TC degradation was showed in Figure 11. As shown in Figure 11a. Under visible light irradiation, CCN and $Bi_{12}O_{17}Cl_2$ can be excited and generate the electrons and holes. The electrons on the CB of $Bi_{12}O_{17}Cl_2$ can be transferred to the CCN due to the CB potential of the $Bi_{12}O_{17}Cl_2$ is negative than the CCN. Simultaneously, holes could be concentrated on the VB of the $Bi_{12}O_{17}Cl_2$. Then the O_2 capture the electrons to form the $\bullet O_2^-$. Then, $\bullet O_2^-$ reacted with H^+ and generated H_2O_2, which was further excited by electrons and changed into •OH. The reactive radicals like •OH and $\bullet O_2^-$

could co-efficiently oxidize pollutant under visible-light irradiation. Also, the holes on the VB of the $Bi_{12}O_{17}Cl_2$ could be degraded pollutant directly. A proposed mechanism of charges separation on CCN/$Bi_{12}O_{17}Cl_2$ was presented in Figure 11b. The charge density surrounding [$Bi_{12}O_{17}$] layer was higher than that of [Cl_2] layer and their electrostatic potential differences was large. This charge distribution between [$Bi_{12}O_{17}$] and [Cl_2] layers in $Bi_{12}O_{17}Cl_2$ would polarize the related atoms to form internal electric field (IEF) along [001] orientation.[40, 70] For pristine $Bi_{12}O_{17}Cl_2$ of numerous [$Bi_{12}O_{17}$] and [Cl_2] layer, the electrons and holes separated by IEF would recombine. The interaction between CCN and $Bi_{12}O_{17}Cl_2$ enhanced the separation and transfer efficiency of photo-generated carriers, which is beneficial for improved the photocatalytic activity of CCN/$Bi_{12}O_{17}Cl_2$ composites.

CONCLUSIONS

In summary, novel CCN/$Bi_{12}O_{17}Cl_2$ photocatalysts were fabricated via the facile ultrasonic chemical method. The CCN/$Bi_{12}O_{17}Cl_2$ composites exhibited outstanding visible light photocatalytic activities toward the degradation of TC. The optimum photocatalytic activity of a CCN/$Bi_{12}O_{17}Cl_2$ sample is approximately 2.3, 1.5, and 32.1 times higher than the activities of pristine $Bi_{12}O_{17}Cl_2$, CCN, and BiOCl, respectively. The enhanced photocatalytic activity could be attributed to the electrostatic interaction between CCN and $Bi_{12}O_{17}Cl_2$. The results of photocurrent response and electrochemical impedance spectroscopy indicated that CCN/$Bi_{12}O_{17}Cl_2$ composite exhibited superior charge transport property. 3D EEMs indicated that the CCN/$Bi_{12}O_{17}Cl_2$ composite has high mineralization ability to TC. Moreover, the roles of $\bullet O_2^-$, h^+ and •OH species in the CCN/$Bi_{12}O_{17}Cl_2$ catalytic system were validated by active species trapping experiments and ESR detection. It can be seen that this study might provide a facile way for construction highly

efficient photocatalyst. Furthermore, the CCN/$Bi_{12}O_{17}Cl_2$ composite can be a candidate that can be used in other refractory pollutant degradation as well as other environmental remediation applications.

ASSOCIATED CONTENT

Supporting Information

XRD, XPS, and FT-IR of the prepared samples and used samples, photocatalytic degradation, cycle runs, and HPLC-MS analysis of TC by the prepared samples.

AUTHOR INFORMATION

Corresponding Authors

*E-mail: zgming@hnu.edu.cn (G.M. Zeng). Tel.:+86-731-88822754.

*E-mail: huangdanlian@hnu.edu.cn (D.L. Huang). Tel.:+86-731-88823701.

ORCID

Guangming Zeng: 0000-0002-4230-7647

Danlian Huang: 0000-0003-4955-5755

Acknowledgements

The authors would like to thank Ying Yan for his assistance with the TEM measurements, Jianjun Zhang for help with SEM measurements, and Shuqu Zhang for his assistance with the DRS measurements. This study was financially supported by the Program for the National Natural Science Foundation of China (51579098, 51779090, 51709101, 51278176, 51521006, 51378190, 51408206), the National Program for Support of Top-Notch Young Professionals of China (2014), the Fundamental Research Funds for the Central Universities, Hunan Provincial Science and Technology Plan Project (No.2016RS3026), the Program for New Century Excellent Talents in University (NCET-13-0186), the Program for Changjiang Scholars and Innovative Research Team in University (IRT-13R17).

References

(1) Zhang, Y.; Zeng, G.-M.; Tang, L.; Huang, D.-L.; Jiang, X.-Y.; Chen, Y.-N. A hydroquinone biosensor using modified core–shell magnetic nanoparticles supported on carbon paste electrode. *Biosensors and Bioelectronics* **2007,** *22* (9-10), 2121-2126, DOI: 10.1016/j.bios.2006.09.030.

(2) Zhang, C.; Lai, C.; Zeng, G.; Huang, D.; Tang, L.; Yang, C.; Zhou, Y.; Qin, L.; Cheng, M. Nanoporous Au-based chronocoulometric aptasensor for amplified detection of Pb 2+ using DNAzyme modified with Au nanoparticles. *Biosensors and Bioelectronics* **2016,** *81*, 61-67.

(3) Wu, H.; Lai, C.; Zeng, G.; Liang, J.; Chen, J.; Xu, J.; Dai, J.; Li, X.; Liu, J.; Chen, M. The interactions of composting and biochar and their implications for soil amendment and pollution remediation: a review. *Critical reviews in biotechnology* **2017,** *37* (6), 754-764.

(4) Zhang, Y.; Zeng, G. M.; Tang, L.; Chen, J.; Zhu, Y.; He, X. X.; He, Y. Electrochemical sensor based on electrodeposited graphene-Au modified electrode and nanoAu carrier amplified signal strategy for attomolar mercury detection. *Analytical chemistry* **2015,** *87* (2), 989-996.

(5) Wan, J.; Zeng, G.; Huang, D.; Hu, L.; Xu, P.; Huang, C.; Deng, R.; Xue, W.; Lai, C.; Zhou, C. Rhamnolipid stabilized nano-chlorapatite: Synthesis and enhancement effect on Pb and Cd-immobilization in polluted sediment. *Journal of hazardous materials* **2018,** *343*, 332-339.

(6) Hu, L.; Wan, J.; Zeng, G.; Chen, A.; Chen, G.; Huang, Z.; He, K.; Cheng, M.; Zhou, C.; Xiong, W. Comprehensive evaluation of the cytotoxicity of CdSe/ZnS quantum dots in Phanerochaete chrysosporium by cellular uptake and oxidative stress. *Environmental Science: Nano* **2017,** *4* (10), 2018-2029.

(7) Lai, C.; Wang, M.-M.; Zeng, G.-M.; Liu, Y.-G.; Huang, D.-L.; Zhang, C.; Wang, R.-Z.; Xu, P.; Cheng, M.; Huang, C. Synthesis of surface molecular imprinted TiO 2/graphene photocatalyst and its highly efficient photocatalytic degradation of target pollutant under visible light irradiation. *Applied Surface Science* **2016,** *390*, 368-376.

(8) Ren, X.; Zeng, G.; Tang, L.; Wang, J.; Wan, J.; Liu, Y.; Yu, J.; H, H.; Ye, S.; Deng, R. Sorption, transport and biodegradation–an insight into bioavailability of persistent organic pollutants in soil. *Science of the Total Environment* **2018,** *610*, 1154-1163.

(9) Xiong, W.; Tong, J.; Yang, Z.; Zeng, G.; Zhou, Y.; Wang, D.; Song, P.; Xu, R.; Zhang, C.; Cheng, M. Adsorption of phosphate from aqueous solution using iron-zirconium modified activated carbon nanofiber: Performance and mechanism. *Journal of colloid and interface science* **2017,** *493*, 17-23.

(10) Schlienger, S.; Alauzun, J.; Michaux, F.; Vidal, L.; Parmentier, J.; Gervais, C.; Babonneau, F.; Bernard, S.; Miele, P.; Parra, J. Micro-, mesoporous boron nitride-based materials templated from zeolites. *Chemistry of Materials* **2011,** *24* (1), 88-96.

(11) Cheng, M.; Zeng, G.; Huang, D.; Lai, C.; Xu, P.; Zhang, C.; Liu, Y. Hydroxyl radicals based advanced oxidation processes (AOPs) for remediation of soils contaminated with organic compounds: A review. *Chemical Engineering Journal* **2016,** *284*, 582-598, DOI: 10.1016/j.cej.2015.09.001.

(12) Xu, P.; Zeng, G. M.; Huang, D. L.; Feng, C. L.; Hu, S.; Zhao, M. H.; Lai, C.; Wei, Z.; Huang, C.; Xie, G. X.; Liu, Z. F. Use of iron oxide nanomaterials in wastewater treatment: A review. *Science of The Total Environment* **2012,** *424*, 1-10, DOI: 10.1016/j.scitotenv.2012.02.023.

(13) Zhang, C.; Lai, C.; Zeng, G.; Huang, D.; Yang, C.; Wang, Y.; Zhou, Y.; Cheng, M. Efficacy of carbonaceous nanocomposites for sorbing ionizable antibiotic sulfamethazine from aqueous solution. *Water Research* **2016,** *95*, 103-112, DOI: 10.1016/j.watres.2016.03.014.

(14) Shao, H.; Zhao, X.; Wang, Y.; Mao, R.; Wang, Y.; Qiao, M.; Zhao, S.; Zhu, Y. Synergetic activation of

peroxymonosulfate by Co3O4 modified g-C3N4 for enhanced degradation of diclofenac sodium under visible light irradiation. *Applied Catalysis B: Environmental* **2017,** *218*, 810-818.

(15) Huang, D.; Hu, C.; Zeng, G.; Cheng, M.; Xu, P.; Gong, X.; Wang, R.; Xue, W. Combination of Fenton processes and biotreatment for wastewater treatment and soil remediation. *Science of the Total Environment* **2017,** *574*, 1599-1610.

(16) Yang, C.; Chen, H.; Zeng, G.; Yu, G.; Luo, S. Biomass accumulation and control strategies in gas biofiltration. *Biotechnology Advances* **2010,** *28* (4), 531-540, DOI: 10.1016/j.biotechadv.2010.04.002.

(17) Huang, D.-L.; Zeng, G.-M.; Feng, C.-L.; Hu, S.; Jiang, X.-Y.; Tang, L.; Su, F.-F.; Zhang, Y.; Zeng, W.; Liu, H.-L. Degradation of lead-contaminated lignocellulosic waste by Phanerochaete chrysosporium and the reduction of lead toxicity. *Environmental Science & Technology* **2008,** *42* (13), 4946-4951, DOI: 10.1021/es800072c.

(18) Zhu, H.; Chen, D.; Li, N.; Xu, Q.; Li, H.; He, J.; Lu, J. Graphene Foam with Switchable Oil Wettability for Oil and Organic Solvents Recovery. *Advanced Functional Materials* **2015,** *25* (4), 597-605, DOI: 10.1002/adfm.201403864.

(19) Zhong, S.; Zhou, C.; Zhang, X.; Zhou, H.; Li, H.; Zhu, X.; Wang, Y. A novel molecularly imprinted material based on magnetic halloysite nanotubes for rapid enrichment of 2, 4-dichlorophenoxyacetic acid in water. *Journal of Hazardous Materials* **2014,** *276*, 58-65.

(20) Huang, D.; Xue, W.; Zeng, G.; Wan, J.; Chen, G.; Huang, C.; Zhang, C.; Cheng, M.; Xu, P. Immobilization of Cd in river sediments by sodium alginate modified nanoscale zero-valent iron: Impact on enzyme activities and microbial community diversity. *Water research* **2016,** *106*, 15-25.

(21) Huang, D.-L.; Wang, R.-Z.; Liu, Y.-G.; Zeng, G.-M.; Lai, C.; Xu, P.; Lu, B.-A.; Xu, J.-J.; Wang, C.; Huang, C. Application of molecularly imprinted polymers in wastewater treatment: a review. *Environmental Science and Pollution Research* **2015,** *22* (2), 963-977.

(22) Huang, D.; Gong, X.; Liu, Y.; Zeng, G.; Lai, C.; Bashir, H.; Zhou, L.; Wang, D.; Xu, P.; Cheng, M. Effects of calcium at toxic concentrations of cadmium in plants. *Planta* **2017**, 1-11.

(23) Huang, D.; Liu, L.; Zeng, G.; Xu, P.; Huang, C.; Deng, L.; Wang, R.; Wan, J. The effects of rice straw biochar on indigenous microbial community and enzymes activity in heavy metal-contaminated sediment. *Chemosphere* **2017,** *174*, 545-553.

(24) Wang, J.; Yang, Z.; Gao, X.; Yao, W.; Wei, W.; Chen, X.; Zong, R.; Zhu, Y. Core-shell g-C 3 N 4 @ZnO composites as photoanodes with double synergistic effects for enhanced visible-light photoelectrocatalytic activities. *Applied Catalysis B: Environmental* **2017,** *217*, 169-180, DOI: 10.1016/j.apcatb.2017.05.034.

(25) Yang, S.; Chen, D.; Li, N.; Xu, Q.; Li, H.; He, J.; Lu, J. Surface-Nanoengineered Bacteria for Efficient Local Enrichment and Biodegradation of Aqueous Organic Wastes: Using Phenol as a Model Compound. *Advanced Materials* **2016,** *28* (15), 2916-2922, DOI: 10.1002/adma.201505493.

(26) Zhou, C.; Li, H.; Zhou, H.; Wang, H.; Yang, P.; Zhong, S. Water‐compatible halloysite‐imprinted polymer by Pickering emulsion polymerization for the selective recognition of herbicides. *Journal of separation science* **2015,** *38* (8), 1365-1371.

(27) Gong, J.-L.; Wang, B.; Zeng, G.-M.; Yang, C.-P.; Niu, C.-G.; Niu, Q.-Y.; Zhou, W.-J.; Liang, Y. Removal of cationic dyes from aqueous solution using magnetic multi-wall carbon nanotube nanocomposite as adsorbent. *Journal of Hazardous Materials* **2009,** *164* (2-3), 1517-1522, DOI: 10.1016/j.jhazmat.2008.09.072.

(28) Cheng, Y.; He, H.; Yang, C.; Zeng, G.; Li, X.; Chen, H.; Yu, G. Challenges and solutions for biofiltration of hydrophobic volatile organic compounds. *Biotechnology Advances* **2016,** *34* (6),

1091-1102, DOI: 10.1016/j.biotechadv.2016.06.007.
(29) Gong, X.; Huang, D.; Liu, Y.; Zeng, G.; Wang, R.; Wan, J.; Zhang, C.; Cheng, M.; Qin, X.; Xue, W. Stabilized Nanoscale Zerovalent Iron Mediated Cadmium Accumulation and Oxidative Damage of Boehmeria nivea (L.) Gaudich Cultivated in Cadmium Contaminated Sediments. *Environmental science & technology* **2017,** *51* (19), 11308-11316.
(30) Pan, M.; Zhang, H.; Gao, G.; Liu, L.; Chen, W. Facet-Dependent Catalytic Activity of Nanosheet-Assembled Bismuth Oxyiodide Microspheres in Degradation of Bisphenol A. *Environmental Science & Technology* **2015,** *49* (10), 6240-6248, DOI: 10.1021/acs.est.5b00626.
(31) Li, K.; Han, M.; Chen, R.; Li, S.-L.; Xie, S.-L.; Mao, C.; Bu, X.; Cao, X.-L.; Dong, L.-Z.; Feng, P.; Lan, Y.-Q. Hexagonal@Cubic CdS Core@Shell Nanorod Photocatalyst for Highly Active Production of H2 with Unprecedented Stability. *Advanced Materials* **2016,** *28* (40), 8906-8911, DOI: 10.1002/adma.201601047.
(32) Li, J.; Wu, X.; Pan, W.; Zhang, G.; Chen, H. Vacancy-Rich Monolayer BiO2−x as a Highly Efficient UV, Visible, and Near-Infrared Responsive Photocatalyst. *Angewandte Chemie* **2018,** *130* (2), 500-504, DOI: 10.1002/ange.201708709.
(33) Li, H.; Shi, J.; Zhao, K.; Zhang, L. Sustainable molecular oxygen activation with oxygen vacancies on the {001} facets of BiOCl nanosheets under solar light. *Nanoscale* **2014,** *6* (23), 14168-14173, DOI: 10.1039/c4nr04810e.
(34) Li, J.; Li, H.; Zhan, G.; Zhang, L. Solar Water Splitting and Nitrogen Fixation with Layered Bismuth Oxyhalides. *Accounts of Chemical Research* **2017,** *50* (1), 112-121, DOI: 10.1021/acs.accounts.6b00523.
(35) Wang, C.-Y.; Zhang, X.; Qiu, H.-B.; Wang, W.-K.; Huang, G.-X.; Yang, J.; Yu, H.-Q. Photocatalytic degradation of bisphenol A by oxygen-rich and highly visible-light responsive Bi12O17Cl2 nanobelts. *Applied Catalysis B: Environmental* **2017,** *200*, 659-665, DOI: 10.1016/j.apcatb.2016.07.054.
(36) Xiao, X.; Jiang, J.; Zhang, L. Selective oxidation of benzyl alcohol into benzaldehyde over semiconductors under visible light: The case of Bi12O17Cl2 nanobelts. *Applied Catalysis B: Environmental* **2013,** *142*, 487-493, DOI: http://dx.doi.org/10.1016/j.apcatb.2013.05.047.
(37) Huang, H.; Xiao, K.; He, Y.; Zhang, T.; Dong, F.; Du, X.; Zhang, Y. In situ assembly of BiOI@Bi12O17Cl2 p-n junction: charge induced unique front-lateral surfaces coupling heterostructure with high exposure of BiOI {001} active facets for robust and nonselective photocatalysis. *Applied Catalysis B: Environmental* **2016,** *199*, 75-86, DOI: 10.1016/j.apcatb.2016.06.020.
(38) He, G.; Xing, C.; Xiao, X.; Hu, R.; Zuo, X.; Nan, J. Facile synthesis of flower-like Bi12O17Cl2/β-Bi2O3 composites with enhanced visible light photocatalytic performance for the degradation of 4-tert-butylphenol. *Applied Catalysis B: Environmental* **2015,** *170-171*, 1-9, DOI: 10.1016/j.apcatb.2015.01.015.
(39) Hao, L.; Huang, H.; Guo, Y.; Du, X.; Zhang, Y. Bismuth oxychloride homogeneous phasejunction BiOCl/Bi12O17Cl2 with unselectively efficient photocatalytic activity and mechanism insight. *Applied Surface Science* **2017,** *420*, 303-312, DOI: http://dx.doi.org/10.1016/j.apsusc.2017.05.076.
(40) Li, J.; Zhan, G.; Yu, Y.; Zhang, L. Superior visible light hydrogen evolution of Janus bilayer junctions via atomic-level charge flow steering. *Nature Communications* **2016,** *7*, 11480, DOI: 10.1038/ncomms11480.
(41) Yang, P.; Ou, H.; Fang, Y.; Wang, X. A Facile Steam Reforming Strategy to Delaminate Layered Carbon Nitride Semiconductors for Photoredox Catalysis. *Angewandte Chemie International Edition* **2017,** *56* (14), 3992-3996, DOI: 10.1002/anie.201700286.

(42) Zheng, D.; Cao, X.-N.; Wang, X. Precise Formation of a Hollow Carbon Nitride Structure with a Janus Surface To Promote Water Splitting by Photoredox Catalysis. *Angewandte Chemie International Edition* **2016,** *55* (38), 11512-11516, DOI: 10.1002/anie.201606102.

(43) Lin, L.; Ou, H.; Zhang, Y.; Wang, X. Tri-s-triazine-Based Crystalline Graphitic Carbon Nitrides for Highly Efficient Hydrogen Evolution Photocatalysis. *ACS Catalysis* **2016,** *6* (6), 3921-3931, DOI: 10.1021/acscatal.6b00922.

(44) Huang, D.; Wang, X.; Zhang, C.; Zeng, G.; Peng, Z.; Zhou, J.; Cheng, M.; Wang, R.; Hu, Z.; Qin, X. Sorptive removal of ionizable antibiotic sulfamethazine from aqueous solution by graphene oxide-coated biochar nanocomposites: Influencing factors and mechanism. *Chemosphere* **2017,** *186*, 414-421.

(45) Deng, Y.; Tang, L.; Zeng, G.; Zhu, Z.; Yan, M.; Zhou, Y.; Wang, J.; Liu, Y.; Wang, J. Insight into highly efficient simultaneous photocatalytic removal of Cr(VI) and 2,4-diclorophenol under visible light irradiation by phosphorus doped porous ultrathin g-C3N4 nanosheets from aqueous media: Performance and reaction mechanism. *Applied Catalysis B: Environmental* **2017,** *203*, 343-354, DOI: 10.1016/j.apcatb.2016.10.046.

(46) Zheng, Y.; Lin, L. H.; Wang, B.; Wang, X. C. Graphitic Carbon Nitride Polymers toward Sustainable Photoredox Catalysis. *Angew. Chem.-Int. Edit.* **2015,** *54* (44), 12868-12884, DOI: 10.1002/anie.201501788.

(47) Wan, Z.; Zhang, G.; Wu, X.; Yin, S. Novel visible-light-driven Z-scheme Bi 12 GeO 20 /g-C 3 N 4 photocatalyst: Oxygen-induced pathway of organic pollutants degradation and proton assisted electron transfer mechanism of Cr(VI) reduction. *Applied Catalysis B: Environmental* **2017,** *207*, 17-26, DOI: 10.1016/j.apcatb.2017.02.014.

(48) Yang, S.-F.; Niu, C.-G.; Huang, D.-W.; Zhang, H.; Liang, C.; Zeng, G.-M. SrTiO 3 nanocubes decorated with Ag/AgCl nanoparticles as photocatalysts with enhanced visible-light photocatalytic activity towards the degradation of dyes, phenol and bisphenol A. *Environmental Science: Nano* **2017,** *4* (3), 585-595.

(49) Wang, K.; Zhang, G.; Li, J.; Li, Y.; Wu, X. 0D/2D Z-Scheme Heterojunctions of Bismuth Tantalate Quantum Dots/Ultrathin g-C3N4 Nanosheets for Highly Efficient Visible Light Photocatalytic Degradation of Antibiotics. *ACS Applied Materials & Interfaces* **2017,** *9* (50), 43704-43715, DOI: 10.1021/acsami.7b14275.

(50) Wei, Z.; Liang, F.; Liu, Y.; Luo, W.; Wang, J.; Yao, W.; Zhu, Y. Photoelectrocatalytic degradation of phenol-containing wastewater by TiO 2 /g-C 3 N 4 hybrid heterostructure thin film. *Applied Catalysis B: Environmental* **2017,** *201*, 600-606, DOI: 10.1016/j.apcatb.2016.09.003.

(51) Jiang, G.; Li, X.; Lan, M.; Shen, T.; Lv, X.; Dong, F.; Zhang, S. Monodisperse bismuth nanoparticles decorated graphitic carbon nitride: Enhanced visible-light-response photocatalytic NO removal and reaction pathway. *Applied Catalysis B: Environmental* **2017,** *205*, 532-540, DOI: 10.1016/j.apcatb.2017.01.009.

(52) Tian, N.; Zhang, Y.; Li, X.; Xiao, K.; Du, X.; Dong, F.; Waterhouse, G. I. N.; Zhang, T.; Huang, H. Precursor-reforming protocol to 3D mesoporous g-C3N4 established by ultrathin self-doped nanosheets for superior hydrogen evolution. *Nano Energy* **2017,** *38*, 72-81, DOI: https://doi.org/10.1016/j.nanoen.2017.05.038.

(53) Dang, K.; Wang, T.; Li, C.; Zhang, J.; Liu, S.; Gong, J. Improved Oxygen Evolution Kinetics and Surface States Passivation of Ni-Bi Co-Catalyst for a Hematite Photoanode. *Engineering* **2017,** *3* (3), 285-289.

(54) Chen, F.; Yang, Q.; Wang, Y.; Zhao, J.; Wang, D.; Li, X.; Guo, Z.; Wang, H.; Deng, Y.; Niu, C.; Zeng, G. Novel ternary heterojunction photcocatalyst of Ag nanoparticles and g-C3N4 nanosheets co-modified BiVO4 for wider spectrum visible-light photocatalytic degradation of refractory pollutant. *Applied Catalysis B: Environmental* **2017,** *205*, 133-147, DOI: 10.1016/j.apcatb.2016.12.017.

(55) Chen, F.; Yang, Q.; Wang, S.; Yao, F.; Sun, J.; Wang, Y.; Zhang, C.; Li, X.; Niu, C.; Wang, D.; Zeng, G. Graphene oxide and carbon nitride nanosheets co-modified silver chromate nanoparticles with enhanced visible-light photoactivity and anti-photocorrosion properties towards multiple refractory pollutants degradation. *Applied Catalysis B: Environmental* **2017,** *209*, 493-505, DOI: 10.1016/j.apcatb.2017.03.026.

(56) Zhang, J.; Wang, T.; Chang, X.; Li, A.; Gong, J. Fabrication of porous nanoflake BiMO x (M= W, V, and Mo) photoanodes via hydrothermal anion exchange. *Chemical science* **2016,** *7* (10), 6381-6386.

(57) Wang, R.; Pan, K.; Han, D.; Jiang, J.; Xiang, C.; Huang, Z.; Zhang, L.; Xiang, X. Solar‐Driven H2O2 Generation From H2O and O2 Using Earth‐Abundant Mixed‐Metal Oxide@ Carbon Nitride Photocatalysts. *ChemSusChem* **2016,** *9* (17), 2470-2479.

(58) Wang, R.; Zhang, X.; Li, F.; Cao, D.; Pu, M.; Han, D.; Yang, J.; Xiang, X. Energy-level dependent H 2 O 2 production on metal-free, carbon-content tunable carbon nitride photocatalysts. *Journal of Energy Chemistry* **2018,** *27* (2), 343-350, DOI: 10.1016/j.jechem.2017.12.014.

(59) Zhou, C. Y.; Lai, C.; Huang, D. L.; Zeng, G. M.; Zhang, C.; Cheng, M.; Hu, L.; Wan, J.; Xiong, W. P.; Wen, M.; Wen, X. F.; Qin, L. Highly porous carbon nitride by supramolecular preassembly of monomers for photocatalytic removal of sulfamethazine under visible light driven. *Applied Catalysis B-Environmental* **2018,** *220*, 202-210, DOI: 10.1016/j.apcatb.2017.08.055.

(60) Wang, C.-Y.; Zhang, X.; Song, X.-N.; Wang, W.-K.; Yu, H.-Q. Novel Bi12O15Cl6Photocatalyst for the Degradation of Bisphenol A under Visible-Light Irradiation. *ACS Applied Materials & Interfaces* **2016,** *8* (8), 5320-5326, DOI: 10.1021/acsami.5b12092.

(61) Zhou, C.; Lai, C.; Xu, P.; Zeng, G.; Huang, D.; Zhang, C.; Cheng, M.; Hu, L.; Wan, J.; Liu, Y.; Xiong, W.; Deng, Y.; Wen, M. In Situ Grown AgI/Bi12O17Cl2 Heterojunction Photocatalysts for Visible Light Degradation of Sulfamethazine: Efficiency, Pathway, and Mechanism. *ACS Sustainable Chemistry & Engineering* **2018,** *6* (3), 4174-4184, DOI: 10.1021/acssuschemeng.7b04584.

(62) Shalom, M.; Inal, S.; Fettkenhauer, C.; Neher, D.; Antonietti, M. Improving Carbon Nitride Photocatalysis by Supramolecular Preorganization of Monomers. *Journal of the American Chemical Society* **2013,** *135* (19), 7118-7121, DOI: 10.1021/ja402521s.

(63) Shao, H.; Zhao, X.; Wang, Y.; Ma, R.; Wang, Y.; Qiao, M.; Zhao, S.; Zhu, Y. Synergetic activation of peroxymonosulfate by Co 3 O 4 modified g-C 3 N 4 for enhanced degradation of diclofenac sodium under visible light irradiation. *Applied Catalysis B: Environmental* **2017,** *218*, 810-818, DOI: 10.1016/j.apcatb.2017.07.016.

(64) Zhang, M.; Luo, W.; Wei, Z.; Jiang, W.; Liu, D.; Zhu, Y. Separation free C 3 N 4 /SiO 2 hybrid hydrogels as high active photocatalysts for TOC removal. *Applied Catalysis B: Environmental* **2016,** *194*, 105-110, DOI: 10.1016/j.apcatb.2016.04.049.

(65) Cui, W.; Li, J.; Dong, F.; Sun, Y.; Jiang, G.; Cen, W.; Lee, S. C.; Wu, Z. Highly efficient performance and conversion pathway of photocatalytic NO oxidation on SrO-clusters@ amorphous carbon nitride. *Environmental science & technology* **2017,** *51* (18), 10682-10690.

(66) Tang, Y.; Wang, R.; Yang, Y.; Yan, D.; Xiang, X. Highly enhanced photoelectrochemical water oxidation efficiency based on triadic quantum dot/layered double hydroxide/BiVO4 photoanodes. *ACS applied materials & interfaces* **2016,** *8* (30), 19446-19455.

(67) Cheng, M.; Zeng, G.; Huang, D.; Lai, C.; Liu, Y.; Xu, P.; Zhang, C.; Wan, J.; Hu, L.; Xiong, W. Salicylic acid–methanol modified steel converter slag as heterogeneous Fenton-like catalyst for enhanced degradation of alachlor. *Chemical Engineering Journal* **2017,** *327*, 686-693.
(68) Cui, W.; Li, J.; Cen, W.; Sun, Y.; Lee, S.; Dong, F. Steering the interlayer energy barrier and charge flow via bioriented transportation channels in g-C3N4: Enhanced photocatalysis and reaction mechanism. *Journal of Catalysis* **2017,** *352*, 351-360.
(69) Xia, J.; Ji, M.; Di, J.; Wang, B.; Yin, S.; Zhang, Q.; He, M.; Li, H. Construction of ultrathin C3N4/Bi4O5I2 layered nanojunctions via ionic liquid with enhanced photocatalytic performance and mechanism insight. *Applied Catalysis B: Environmental* **2016,** *191*, 235-245, DOI: 10.1016/j.apcatb.2016.02.058.
(70) Bai, Y.; Ye, L.; Wang, L.; Shi, X.; Wang, P.; Bai, W.; Wong, P. K. gC 3 N 4/Bi 4 O 5 I 2 heterojunction with I 3−/I− redox mediator for enhanced photocatalytic CO 2 conversion. *Applied Catalysis B: Environmental* **2016,** *194*, 98-104.

Figure captions:

Figure 1 SEM images of samples $Bi_{12}O_{17}Cl_2$ (a), CCN (b), CCN/$Bi_{12}O_{17}Cl_2$ (c-d), and corresponding elemental maps of CCN/$Bi_{12}O_{17}Cl_2$ (e to i).

Figure 2 TEM images of CCN (a), $Bi_{12}O_{17}Cl_2$ (b), CCN/$Bi_{12}O_{17}Cl_2$ (c), and HRTEM images of CCN/$Bi_{12}O_{17}Cl_2$ (d).

Figure 3 (a) XRD patterns of samples CCN, $Bi_{12}O_{17}Cl_2$, and CCN/$Bi_{12}O_{17}Cl_2$ (5%, 10%, and 20%); (b) FT-IR Spectra of samples CCN, $Bi_{12}O_{17}Cl_2$, and CCN/$Bi_{12}O_{17}Cl_2$.

Figure 4 The XPS spectra of CCN/$Bi_{12}O_{17}Cl_2$ (a) survey spectra, (b) high resolution Bi 4f, (c) high resolution O 1s, (d) high resolution Cl 2p, (e) high resolution C1s, and (c) high resolution N1s.

Figure 5 (a) UV-vis adsorption spectra of samples, and (b) The plots of $(\alpha hv)^{1/2}$ *vs* photon energy *(hv)* for $Bi_{12}O_{17}Cl_2$ and the plots of $(\alpha hv)^2$ *vs* photon energy *(hv)* for CCN.

Figure 6 (a) Photocurrent transient measurement and (b) electrochemical impedance spectra of photocatalysts.

Figure 7 (a) Photodegradation rate of TC on different photocatalyst, **(b)** effects of initial concentration of **TC on** CCN/$Bi_{12}O_{17}Cl_2$**.**

Figure 8 3D EEMs of the aqueous solution: (a) taken from the original solution; (b) collected after 60 min adsorption in dark; and (c−f) obtained after an irradiation time of 30, 60, 80 and 120 min, respectively.

Figure 9 Photocatalytic activities of the CCN/$Bi_{12}O_{17}Cl_2$ (a and b) for degradation of TC under visible light irradiation in the presence of trapping systems. ESR spectra of $Bi_{12}O_{17}Cl_2$ and CCN/$Bi_{12}O_{17}Cl_2$ dispersion under both the dark and visible light irradiation (> 420 nm) condition:

(c) in methanol dispersion for DMPO-•$\mathbf{O_2^-}$, (d) in aqueous dispersion for DMPO-•OH.

Figure 10 (a) Mott–Schottky plots of pure CCN and $Bi_{12}O_{17}Cl_2$ film electrodes at frequency of 1000 Hz in an aqueous solution of Na_2SO_4 (0.1 M); (b) valence band XPS spectra of pure CCN and $Bi_{12}O_{17}Cl_2$.

Figure 11 Proposed Charge Separation Process in the CCN/$Bi_{12}O_{17}Cl_2$ heterostructures under Visible Light Irradiation (a-b).

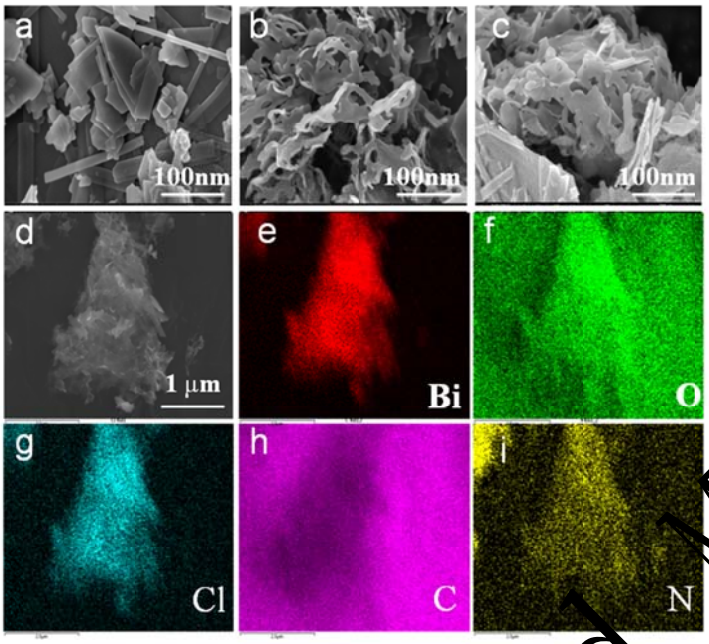

Figure 1. SEM images of samples $Bi_{12}O_{17}Cl_2$ (a), CCN (b), CCN/$Bi_{12}O_{17}Cl_2$ (c-d), and corresponding elemental maps of CCN/$Bi_{12}O_{17}Cl_2$ (e to i).

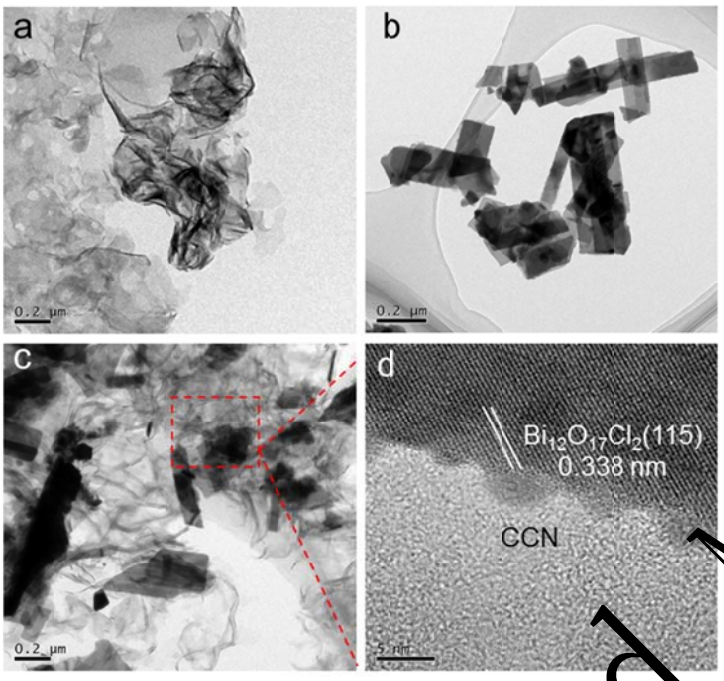

Figure 2 TEM images of CCN (a), $Bi_{12}O_{17}Cl_2$ (b), CCN/$Bi_{12}O_{17}Cl_2$ (c), and HRTEM images of CCN/$Bi_{12}O_{17}Cl_2$ (d).

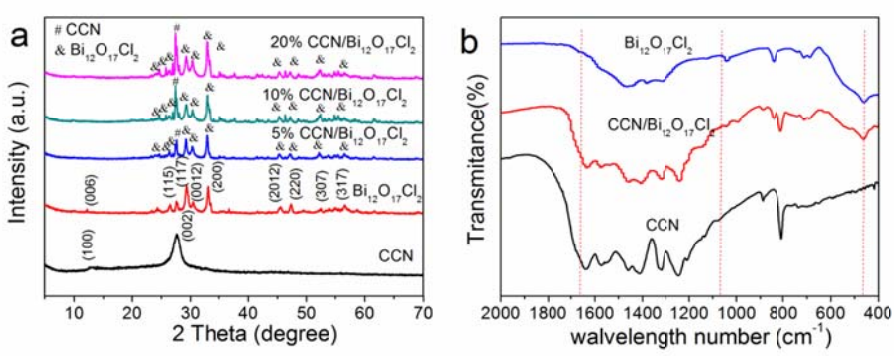

Figure 3. (a) XRD patterns of samples CCN, $Bi_{12}O_{17}Cl_2$, and CCN/$Bi_{12}O_{17}Cl_2$ (5%, 10%, and 20%); (b) FT-IR Spectra of samples CCN, $Bi_{12}O_{17}Cl_2$, and CCN/$Bi_{12}O_{17}Cl_2$.

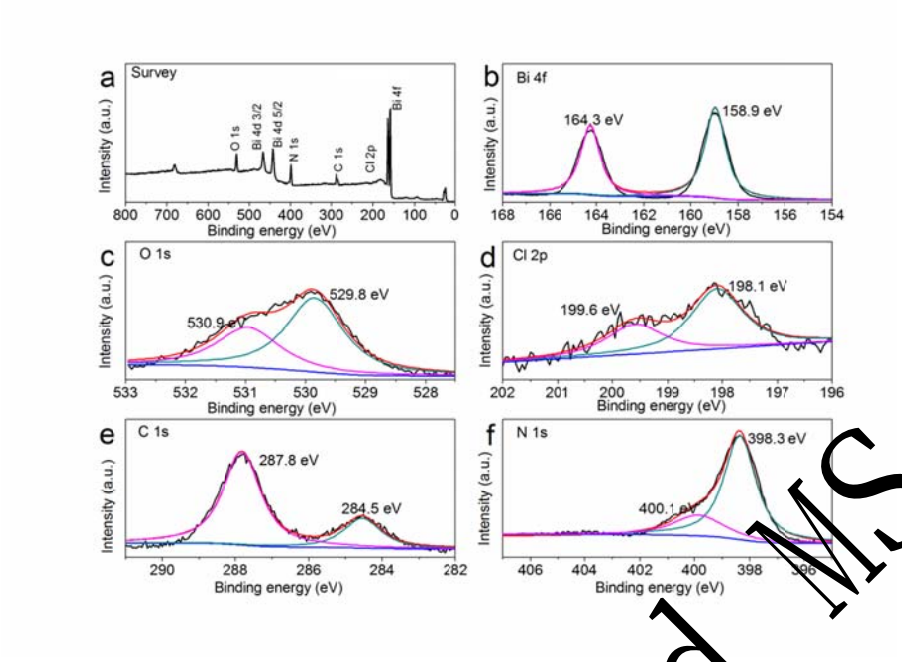

Figure 4. The XPS spectra of CCN/$Bi_{12}O_{17}Cl_2$ (a) survey spectra, (b) high resolution Bi 4f, (c) high resolution O 1s, (d) high resolution Cl 2p, (e) high resolution C1s, and (c) high resolution N1s.

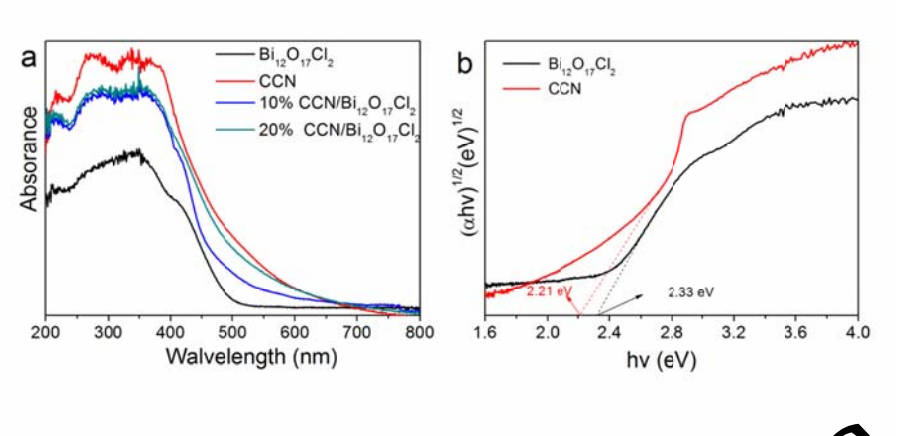

Figure 5. (a) UV-vis adsorption spectra of samples, and (b) The plots of $(\alpha hv)^{1/2}$ *vs* photon energy *(hv)* for $Bi_{12}O_{17}Cl_2$ and the plots of $(\alpha hv)^2$ *vs* photon energy *(hv)* for CCN.

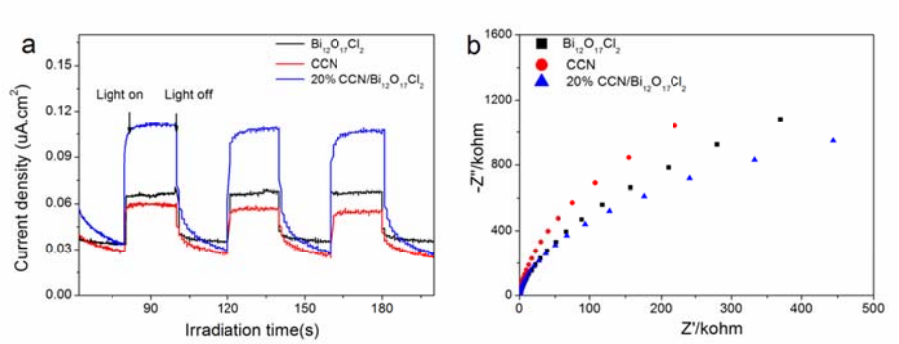

Figure 6. (a) Photocurrent transient measurement and (b) electrochemical impedance spectra of photocatalysts.

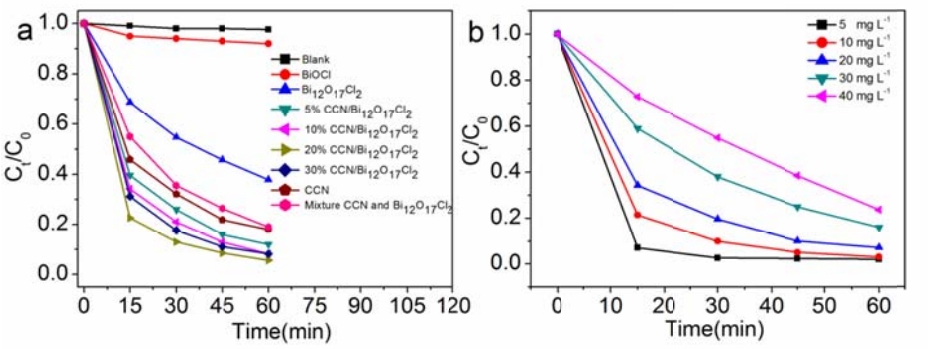

Figure 7. (a) Photodegradation rate of TC on different photocatalyst, **(b)** effects of initial concentration of **TC on** CCN /$Bi_{12}O_{17}Cl_2$**.**

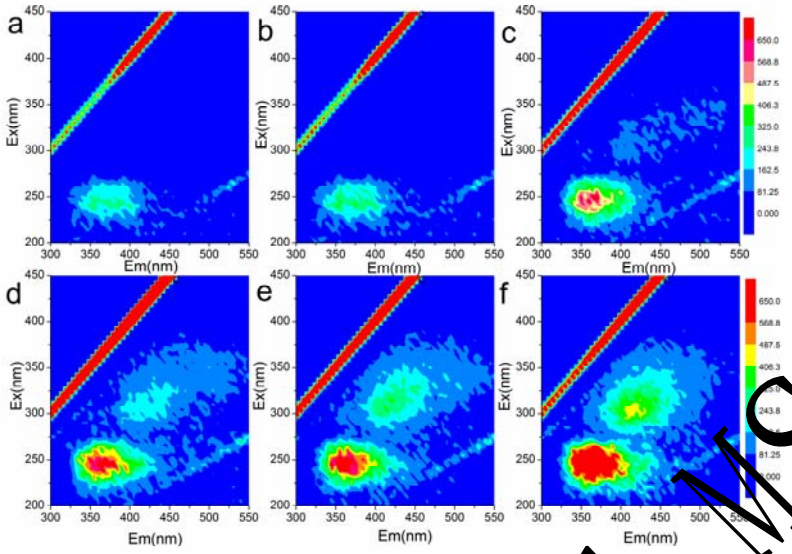

Figure 8 3D EEMs of the aqueous solution: (a) taken from the original solution; (b) collected after 60 min adsorption in dark; and (c−f) obtained after an irradiation time of 30, 60, 80 and 120 min, respectively.

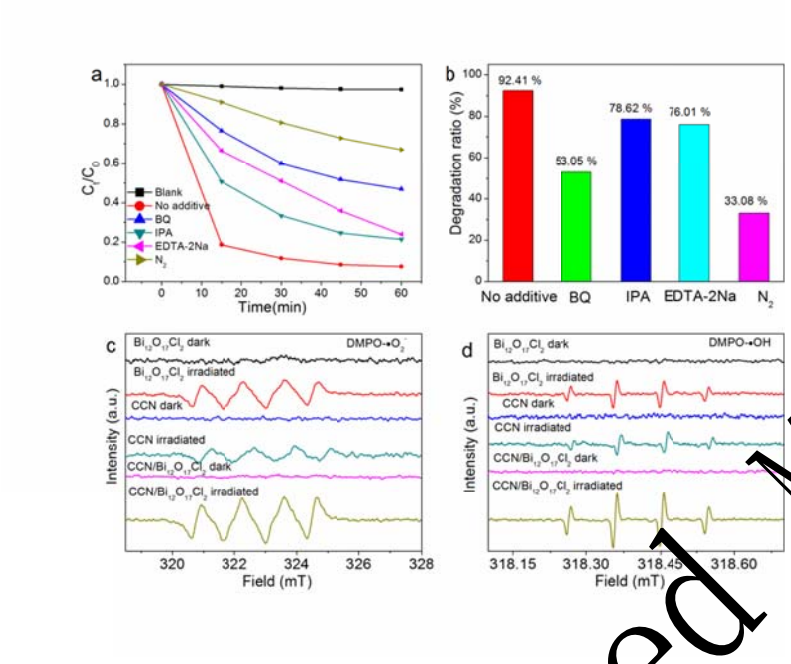

Figure 9. Photocatalytic activities of the CCN/$Bi_{12}O_{17}Cl_2$ (a) and (b) for degradation of TC under visible light irradiation in the presence of trapping systems. ESR spectra of $Bi_{12}O_{17}Cl_2$ and CCN/$Bi_{12}O_{17}Cl_2$ dispersion under both the dark and visible light irradiation (> 420 nm) condition: (c) in methanol dispersion for DMPO-•O_2^-, (d) in aqueous dispersion for DMPO-•OH.

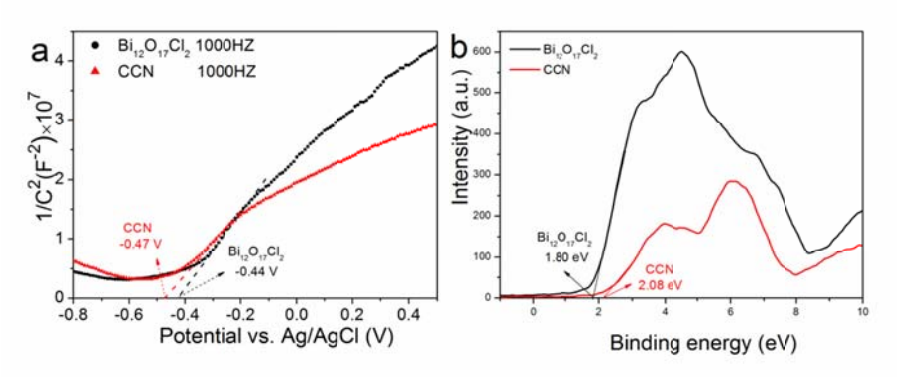

Figure 10. (a) Mott–Schottky plots of pure CCN and $Bi_{12}O_{17}Cl_2$ film electrodes at frequencies of 1000 Hz in an aqueous solution of Na_2SO_4 (0.1 M); (b) valence band XPS spectra of pure CCN and $Bi_{12}O_{17}Cl_2$.

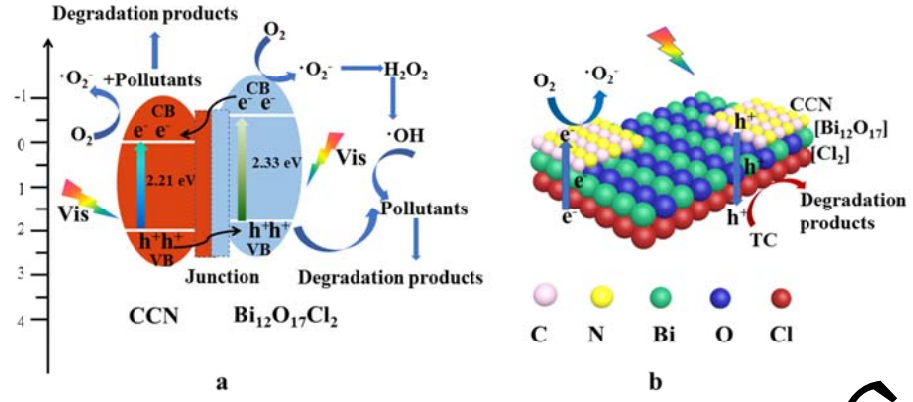

Figure 11. Proposed Charge Separation Process in the CCN/$Bi_{12}O_{17}Cl_2$ heterostructures under Visible Light Irradiation (a-b).

Table 1 Pseudo-First-Order Rate Constants (kapp) and Degradation Efficiencies for the TC in Different Photocatalytic Systems

Catalyst	$K_{app}(min^{-1})$	Degradation Efficiencies (%)
BiOCl	0.0013	8.1
$Bi_{12}O_{17}Cl_2$	0.0157	62.2
5% CCN/$Bi_{12}O_{17}Cl_2$	0.0343	88
10% CCN/ $Bi_{12}O_{17}Cl_2$	0.0397	91.8
20% CCN/ $Bi_{12}O_{17}Cl_2$	0.0409	94
30% CCN/ $Bi_{12}O_{17}Cl_2$	0.0402	91.8
Mixture	0.027	81.9
CCN	0.0278	80.9